JOURNAL OF MATERIALS SCIENCE 26 (1991) 6553–6564

Fracture toughness evaluation for short glass fibre reinforced composites

C. L. CHOW, T. J. LU*
Department of Mechanical Engineering, Southern Illinois University at Edwardsville, Edwardsville, IL 62026-1805, USA

Valid plane-stress fracture toughness evaluation of short fibre reinforced composites relies essentially on the successful separation of the energy absorbed in the localized crack-tip region out of the total energy absorbed by the cracked material body at large. Three different experimental techniques, all stemming from the energetic interpretation of the J integral, are utilized and their relative merits in the characterization of fracture initiation in short glass fibre reinforced injection-moulded nylon 6.6 examined. Various theoretical aspects concerning these experimental methods are outlined. The rationale behind using a single-edge-notched tension type specimen for the J_c test is presented. The J_c value obtained from the compliance calibration method and the quasistatic energy method agree closely and can be considered to be independent of pre-crack length and specimen geometry when the pre-crack length to specimen width ratio (a/w) is larger than 0.45. The extrapolation method fails nevertheless to yield a physically consistent J_c value, possibly due to its questionable theoretical representation. As no constraint on boundary conditions is necessitated during the course of crack extension, the quasistatic energy is physically more appealing.

1. Introduction

Like most metallic engineering materials, short fibre reinforced thermoplastic composites (SFC) which often contain crack-like defects have been characterized primarily in the past using linear elastic fracture mechanics [1–5]. Practical difficulties have, however, frequently been encountered in accurately analysing the crack tip region due to the heterogeneous nature of composite materials. Moreover, the large specimen thickness required to produce an essentially plane strain type fracture is not desirable, especially for injection-moulded plastic products. Also, the presence of non-linear elastic–plastic behaviour, as a result of several energy dissipative mechanisms on the microscopic scale such as matrix cracking and, fibre–matrix interface debonding [6, 7], complicates the problem significantly. Consequently, it has been advocated recently that attention should not be focused on the small crack-tip region where the material continuity condition may have been violated by these microstructural irreversible occurrences. The global energy balance approach proposed initially by Griffith [8, 9] for crack instability in brittle fractures, on the other hand, when suitably modified to take into account the influence of substantial irreversible deformation behaviours preceding crack initiation, can possibly be a more useful method in determining experimentally the specific essential work of fracture required to produce a new unit surface area.

Among several methods for measuring fracture toughness values in the presence of extensive crack-tip plastic yield – the crack growth resistance curve (R-curve), the crack opening displacement (COD), the J integral and the non-linear energy method ($\tilde{G}$-method) proposed by Liebowitz and Eftis [10], the path independent J integral introduced by Rice [11–13] has been assumed to be capable of providing a suitable parameter for characterizing the fracture behaviour of SFC. Microcracks at the fibre–matrix interface and at the fibre end appear at very low load levels due to the large stress concentrations produced by the "stiff" fibres [6, 7]. This subcritical damage initiation and propagation prior to fracture may invalidate the hypothesis of the path-independence nature of J.

Agarwal *et al.* [14] first explored the possibility of using J integral as a fracture criterion for a randomly oriented short glass fibre reinforced epoxy resin with an average fibre length of 50 mm. In that paper, besides the standard compliance J method, an attempt was made to circumvent the energy dissipation due to microcracking at fibre–matrix interfaces as well as at fibre ends away from the crack tip region by an extrapolation method. The J_c value thus evaluated was found to be approximately independent of crack length when the crack length to single-edge-notched specimen width ratio (a/w) was larger than 0.35. Singh and Parikar [15] employed the same approach to study the fracture behaviour of a polycarbonate thermoplastic and a similar result to that reported in Reference 14 was obtained.

More recently, however, Kim and Joe [16, 17] concluded that the extrapolation method is inherently

* *Permanent address*: Xian Jiaotong University, Xian, China.

0022–2461/91 $03.00 + .12

associated with a subjective judgement. In an effort to separate the essential energy for crack initiation from the energy dissipated due to remote irreversible occurrences, this method extrapolates energy down to the zero length specimen as the energy to be used for crack separation without being aware of the fact that the so-obtained energy is nothing more than the difference in the absorbed energy between a cracked and an uncracked specimen under otherwise identical loading conditions. Practically, Kim and Joe [16, 17] and Chow *et al.* [18] reported that the extrapolation approach could not even yield physically consistent critical J-integral values for both thermoplastic rubber, manufactured by the Monsanto Chemical Company, and carbon black reinforced rubber supplied by the Uniroyal–Goodrich Company. Specifically, it has been found [16, 17] that the extrapolated strain energies to the zero specimen length exhibited frequently negative values which should not have occurred. Kim and Joe have instead proposed to use the so-called "locus method", which measures the critical J integral value from the area enclosed by two loading curves corresponding to two different initial crack lengths and the crack initiation locus. This method relies essentially on the energy release rate interpretation of the J integral and successful use has been reported in the case of thermoplastic rubber as well as polycarbonate [16, 17]. In the absence of irreversible deformations, the locus method is considered as a special case of the more general quasistatic energy method [18–23] which has been demonstrated, both analytically and experimentally, as a valuable approach in fracture studies involving both linear and non-linear elastic structural behaviours.

In this paper, we present some results on measuring the essential fracture energy required to form a new unit surface area in short glass fibre reinforced injection-moulded nylon 6.6 under essentially plane stress condition. Three different experimental techniques are considered, namely, compliance calibration, extrapolation and the quasistatic energy method. Various theoretical aspects concerning these techniques are discussed and grouped together in the ensuing sections. Global energy balance view is employed. Experimental details as well as test results are next reported and compared. Our final objective is to identify a reliable and yet simple means of measuring the fracture toughness of SFC materials.

2. Theoretical developments of experimental techniques

2.1. Rationale behind using edge-notched tension specimen for fracture toughness evaluation of SFC

According to the energetic interpretation of J-contour integral given by Rice [11], at fracture initiation

$$J_c = -\frac{d}{da}(W_{ext} + W_{el}) = 2\gamma + \frac{dW_{pl}}{da} = 2\gamma + J_p \approx J_p \quad (1)$$

where W_{ext} denotes the potential energy of the loading system, W_{el} the elastic strain energy of the cracked body, J_p the plastic dissipation rate which is defined as the energy dissipated irreversibly by plastic deformation during a unit crack extension and γ the true surface energy density. As J_c is considered intrinsic material property and is accordingly required to be a constant, the plastic dissipation rate at fracture initiation, J_p, must also be a constant, at least for variations in the extent of crack-tip plastic yield in a given specimen geometry with its own implied degree of in-plane biaxiality. On the other hand, Liu [24, 25] argued that since the total dissipated plastic deformation energy W_{pl} was a linear function of the volume of crack-tip yield zone with linear size r_p and the volume of the yield zone was proportional to the square of r_p or equivalently the square of crack length a, one immediately obtained from the global energy balance condition of Equation 1 that

$$J_c \approx J_p = \frac{dW_{pl}}{da} = Ma \quad (2)$$

where M is a proportional parameter. Equation 2 will generally invalidate the constant J_c requirement unless large scale crack-tip plastic deformation is constrained by specimen size or geometry such that the proportional parameter M is in itself proportional to the inverse of crack length a. As a matter of fact, for plane strain condition, it has been demonstrated [26] that the J dominated or HRR (Hutchinson–Rice–Rosengren) crack-tip fields [27, 28] remain valid in bending whilst permitting an extent of plasticity comparable to gross yield whereas they become invalid in the centre-cracked version for an extent not far beyond the ASTM limit for the SSY condition of $r_p < 0.02$ (B or b), where B and b are thickness and uncracked ligament of the specimen, respectively. This clearly puts an extremely stringent criterion for the validity of J_c tests using centre-cracked (or edge-cracked) tension specimens, especially in the case of ductile materials where extensive crack-tip blunting as well as necking controlled by large strain occur before the crack starts to propagate (Fig. 1c).

Most short fibre reinforced composites are considered brittle materials. The stiff fibres induce the major portion of plastic deformation and irreversible energy is mostly dissipated through several damage mechanisms such as microscopic matrix cracking at fibre ends and fibre–matrix interface debonding. Fibre breakage is rarely observed on fractured surfaces. This is in sharp contrast with the case of ductile materials where energy is predominantly dissipated through plastic flow associated with the changes in position of the dislocation through lattice structure causing permanent geometrical changes in the shape of the material body (Fig. 1c). As schematically illustrated in Fig. 1b, brittle type microdamages in SFC are controlled essentially by stress, similar to the crazing phenomenon observed in brittle polymers (Fig. 1a). Typical crack-tip microdamages in a single-edge-notched tension specimen made from short glass fibre reinforced injection-moulded nylon 6.6 (see the next section for experimental details) are shown in Figs 2

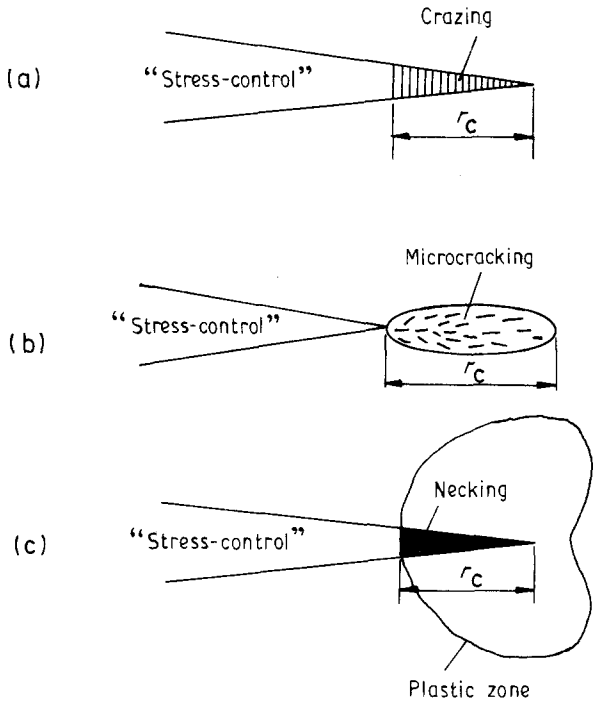

Figure 1 Typical crack tip deformation zones in (a) brittle, (b) SFC and (c) ductile polymeric materials.

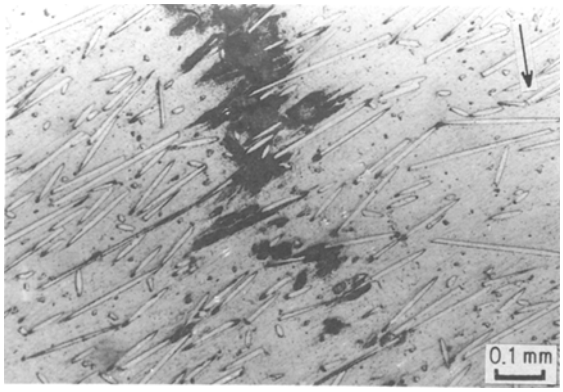

Figure 2 Crack tip damage zone observed under a conventional reflection optical microscope. The arrow shows the crack propagation direction.

and 3 which are observed under both optical microscope and scanning electron microscope (SEM). These micrographs show that the crack follows an irregular, zigzag path which avoids agglomerated fibre groups as much as possible. Similar crack extension patterns have been observed by Mandell *et al.* [6] for several other SFC materials. Microcracking at fibre ends as well as fibre–matrix interface debonding are clearly revealed by the SEM micrograph because those microdefects are not accessible to the evaporated gold–palladium coating and hence act as sites of electrostatic charging. Higher magnification observation of microcrack formation near fibre end and shear crack formation along the fibre–matrix interface is shown in Fig. 4. In fact, interfacial debonding follows from the fibre-end microcracking. Based on the morphology of general fractured surface (Fig. 5), it is believed that interface debonding and fibre pull-out comprise the major mechanism of crack propagation

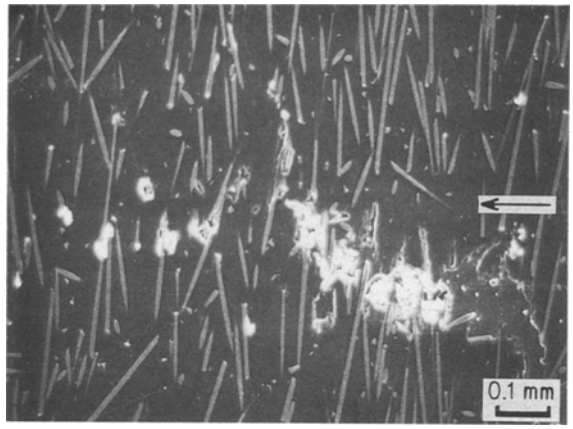

Figure 3 Crack tip damage zone observed by SEM: notice microcracking at fibre ends and fibre–matrix interfacial debonding ahead of the crack tip. The arrow shows the crack propagation direction.

for this material. It seems reasonable that fibre ends become the first sites for damage initiation and propagation. This is expected especially for fibres whose ends are close to the main crack plane. Crack extension under these circumstances may simply occur by growth and coalescence of these microdamages with each other and the main crack. Generally, yielding and necking requiring necessarily large deformations in all cases are observed to be insignificant and negligible.

As a result of large stress concentrations produced by the stiff fibres, microcracking and fibre–matrix interface debonding occur at very low load level and cause the non-linear stress–strain behaviour shown in Fig. 6. Regression analysis of experimental data shows that the stress–strain curve can be described quite accurately by the following Ramberg–Osgood strain-hardening relation

$$\frac{\sigma}{\sigma_0} = \left(\frac{\varepsilon}{\varepsilon_0}\right)^{0.89} \tag{3}$$

where $\sigma_0 = 40$ MPa and $\varepsilon_0 = 0.5\%$ represent, respectively, yield stress and yield strain of the composite with initial Young's modulus equal to 8 GPa.

Based on the foregoing discussions concerning the essentially brittle type fracture behaviours of SFC, it appears to be justified to consider the crack-tip region of a single-edge-notched tension specimen made from SFC as consisting of three distinct characteristic areas (Fig. 7). They are, respectively, the strip-like "process zone", close to the crack tip and lying along the crack line, where the composite is weakened significantly by a cloud of microdefects; an intermediate zone with r_p designating roughly its "radius" in which the small-strain continuum solution will provide a good approximation to the stress and deformation fields; and the outermost region for which the standard elastic asymptotic fields are appropriate. Although the "process zone" is still not well defined and characterized, characterization of material deformations within the intermediate zone has been extensively investigated both theoretically and numerically. For the present boundary value problem, the HRR near-tip singularity fields are generally considered to be an accurate

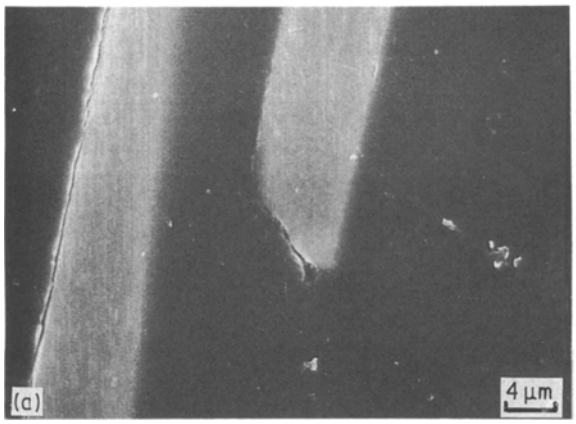

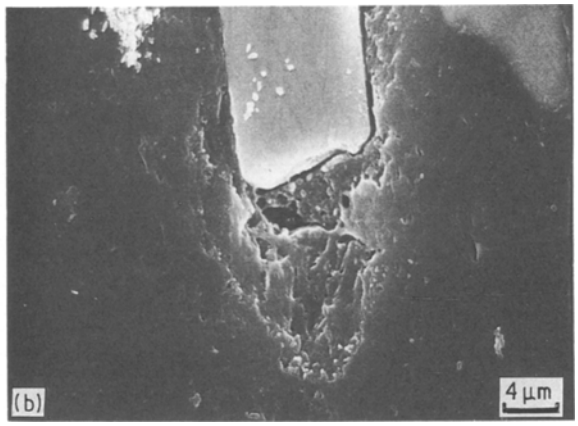

Figure 4 High magnification SEM micrographs of (a) microcracking and interfacial shear cracking, (b) microvoiding at fibre end and (c) fibre–matrix interfacial debonding.

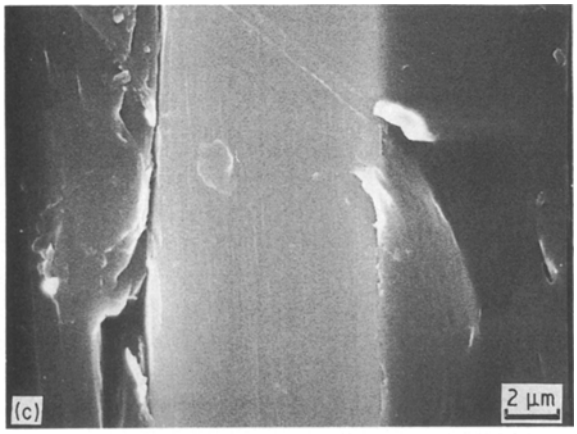

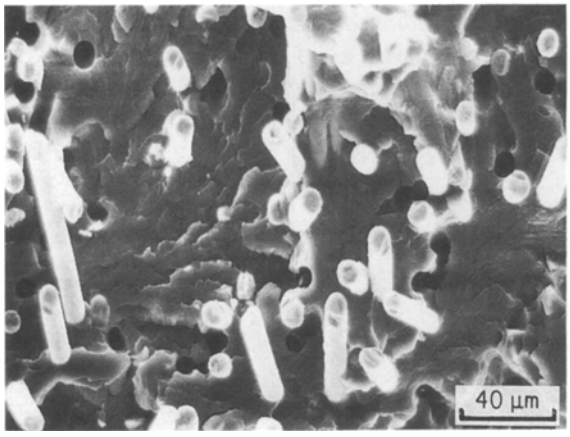

Figure 5 General fractured surface of a single-edge-notched SFC tensile testing specimen.

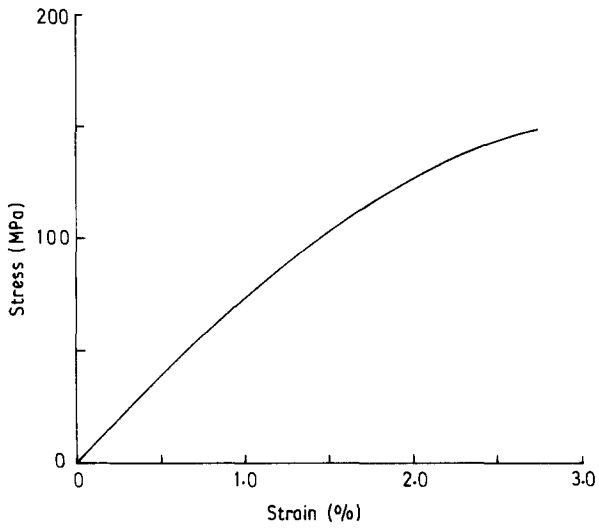

Figure 6 Tensile stress–strain relationship for short glass fibre reinforced nylon 6.6 (Zytel 70G 33 HS1-L) at room temperature, strain rate = 5 mm min^{-1}.

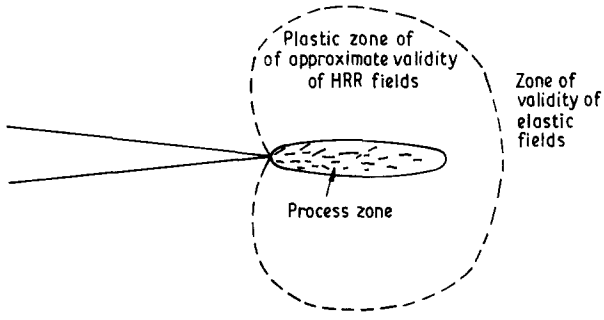

Figure 7 Schematic of crack tip region for a single-edge-notched SFC tensile testing specimen.

solution which can be written as

$$\left.\begin{aligned}
\sigma_{ij} &= \sigma_0\left(\frac{J}{\alpha\sigma_0\varepsilon_0 I_n r}\right)^{1/(n+1)}\tilde{\sigma}_{ij}(\theta, n)\\
\varepsilon_{ij} &= \alpha\varepsilon_0\left(\frac{J}{\alpha\sigma_0\varepsilon_0 I_n r}\right)^{n/(n+1)}\tilde{\varepsilon}_{ij}(\theta, n)\\
u_i &= \frac{J}{I_n\sigma_0}\left(\frac{\alpha\sigma_0\varepsilon_0 I_n r}{J}\right)^{1/(n+1)}\tilde{u}_i(\theta, n)
\end{aligned}\right\} \quad (4)$$

where mode I tensile opening has been assumed and the material satisfies the Ramberg–Osgood type uniaxial stress–strain relation of Equation 3. α and n are material characteristics with n being usually called the strain hardening parameter which, according to Equation 3, is equal to 1/0.89 or 1.12 for the present composite. The dimensionless θ-variations $\tilde{\sigma}_{ij}$, $\tilde{\varepsilon}_{ij}$ and $\tilde{u}_i$ and the normality constant I_n depend on n as well as on whether plane strain or plane stress is assumed. These plastic-singular fields are enclosed by the outer

elastic fields in the form

$$\sigma_{ij} = \frac{K}{(2\pi r)^{1/2}}\tilde{\sigma}_{ij}^{0}(\theta) + \cdots$$
$$\varepsilon_{ij} = \frac{K}{(2\pi r)^{1/2}}\tilde{\varepsilon}_{ij}^{0}(\theta) + \cdots \quad (5)$$
$$u_i = \frac{K}{2\mu}\left(\frac{r}{2\pi}\right)^{1/2}\tilde{u}_i^{0}(\theta) + \cdots$$

where K is the elastic stress intensity factor, $\tilde{\sigma}_{ij}^{0}$, $\tilde{\varepsilon}_{ij}^{0}$ and $\tilde{u}_i^{0}$ are universal functions depending only on the polar angle θ with μ designating the shear modulus. Due to the brittle nature of the composite with n equal to 1.12, it can be observed from Equations 4 and 5 that the intermediate HRR fields do not deviate significantly from the outer elastic fields. This may be true even when the linear elastic condition has been violated. Indeed, with the aid of finite element method (FEM), Liu *et al.* [29–31] studied the plane-stress crack tip fields in four different specimen geometries, namely, a centre-cracked tensile panel, a double-edge-cracked tensile panel, a single-edge-cracked tensile panel, and an edge-cracked bend specimen, which are all made of a typical ductile material – HY 80 steel. Their results for small scale yielding and general yielding coincide very well indicating the existence of a direct correspondence between the crack tip field in SSY and that in general yielding. Furthermore, the direct correspondence also exists between the crack tip fields of a small specimen in general yielding and a large specimen in SSY in all four of the above captioned specimen types [32]. The HRR crack tip fields of Equation 4 agree well with the plane-stress FEM calculations whereas the characteristics of the crack tip fields in plane-strain depend strongly on specimen type as well as loading level [31]. It is, therefore, reasonable to infer that a single-edge-cracked tensile specimen is capable of providing a reliable measure of plane-stress fracture toughness for SFC materials, provided that the crack length to specimen width ratio (a/w) is sufficiently large so that energy dissipation is confined to the localized crack tip region and no remote energy dissipation mechanism exists.

Now assume that irreversible energy dissipated in the localized intermediate plastic zone and in the process zone is controlled completely by elastic deformations of the outermost material body so that

$$W_{pl} = \xi W_{el} \quad (6)$$

where ξ is a proportional constant. At fracture initiation, Equation 6 can be rewritten under plane stress condition as

$$J_p = \xi\left|\frac{dW_{el}}{da}\right| = \xi\frac{\sigma_f^2\pi a(1+\nu)}{2E}(\kappa+1)$$
$$= \xi\frac{2\sigma_f^2\pi a}{E} \quad (7)$$

where σ_f is the fracture stress, E Young's modulus and $\kappa = (3-4\nu)$ but equals $(3-\nu)/(1+\nu)$ under plane strain (ν, Poisson's ratio). Substituting Equation 7 into Equation 1 and applying Clapeyron's theorem, one has

$$\left|\frac{dW_{el}}{da}\right| = 2\gamma + \xi\left|\frac{dW_{el}}{da}\right| \quad (8a)$$

or

$$\sigma_f = \left(\frac{E\gamma}{\pi a(1-\xi)}\right)^{1/2} \quad (8b)$$

With Equation 8b, Equation 7 can be changed into

$$J_p = \frac{2\xi\gamma}{1-\xi} = \frac{2\gamma}{1/\xi - 1} \quad (9)$$

and the fracture toughness of the material becomes

$$J_c = 2\gamma + J_p = \frac{2\gamma}{1-\xi} \quad (10)$$

Obviously, from Equation 7, the proportional parameter M defined in Equation 2 is

$$M = \xi\frac{2\sigma_f^2\pi}{E} \quad (11)$$

If, therefore, ξ is a constant independent of crack length a, it follows from Equations 8b and 11 that M will be inversely proportional to a such that the plastic dissipation rate J_p becomes a constant. The magnitude of ξ, being dependent on the exact form of the stress–strain relation, cannot exceed unity, as the plastic energy dissipation is otherwise larger than its "supplier", i.e., the elastic strain energy release rate. The assumption of constant ξ is illustrated schematically in Fig. 8 where the importance of the true surface energy term 2γ in controlling fracture initiation can be clearly seen, even though its absolute value may be of negligible significance compared with the irreversible term J_p.

In what follows, three different methods of measuring J_c values are briefly outlined. They all depend strongly on the energetic meaning of J_c expressed by Equation 1.

2.2. Compliance calibration method

The first method was first proposed by Begley and Landes [12, 13] and was later known as the compliance J determination. Its essence is outlined as follows.

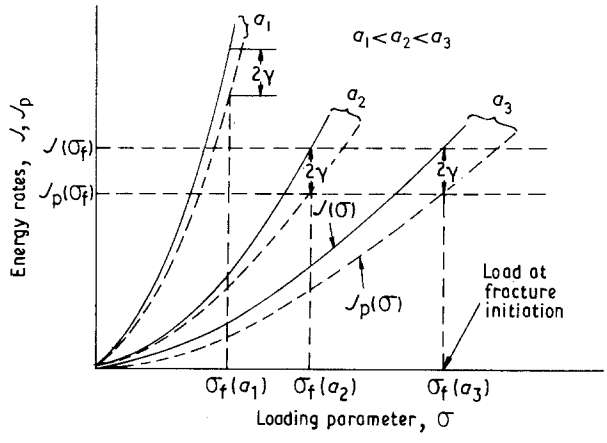

Figure 8 Schematic illustration of constant ξ assumption at fracture initiation when the crack length to specimen width ratio (a/w) exceeds certain threshold value.

1. Bodies with the same in-plane geometrical configurations as well as dimensions are pre-cracked to different crack lengths, Fig. 9a.

2. Displacements being prescribed as boundary conditions, the potential energy ($W_{ext} + W_{el}$) then becomes equal to the integral of the strain energy density which is simply equal to the work done on the body, Fig. 9b.

3. At a given displacement, potential energies of bodies with different crack lengths are obtained by finding areas under corresponding load against load point displacement records, Fig. 9b.

4. J is obtained by finding the slope of the potential energy against crack length plot, Fig. 9c.

5. The final plot is J against the applied load point displacement. If the applied displacement is found for fracture initiation, the critical J value, J_c, can thus be determined from this final plot, Fig. 9d.

2.3. Extrapolation method

This method was developed by Agarwal *et al.* [14] who then encountered some difficulties in attaining consistent J_c values independent of crack length and specimen geometry. Firstly, at fracture initiation, potential energies possessed by bodies with different crack lengths are plotted against specimen lengths (Fig. 10a). The total energy absorbed by a cracked body may be considered as consisting of the energies absorbed in the localized crack tip region and the region away from it; the first portion of the total absorbed energy depends on crack length but not on specimen length whereas the remote energy absorption depends upon the specimen length. It is then assumed that the intercept on the ordinate obtained by extrapolation of straight line in Fig. 10a is the energy absorbed in the crack tip region alone. Energies thus obtained for different crack lengths (Fig. 10b) are assumed to correspond to the same critical load point displacement and as such the slope of the straight line shown in Fig. 10b may be used to obtain J_c value being independent of crack length and specimen length.

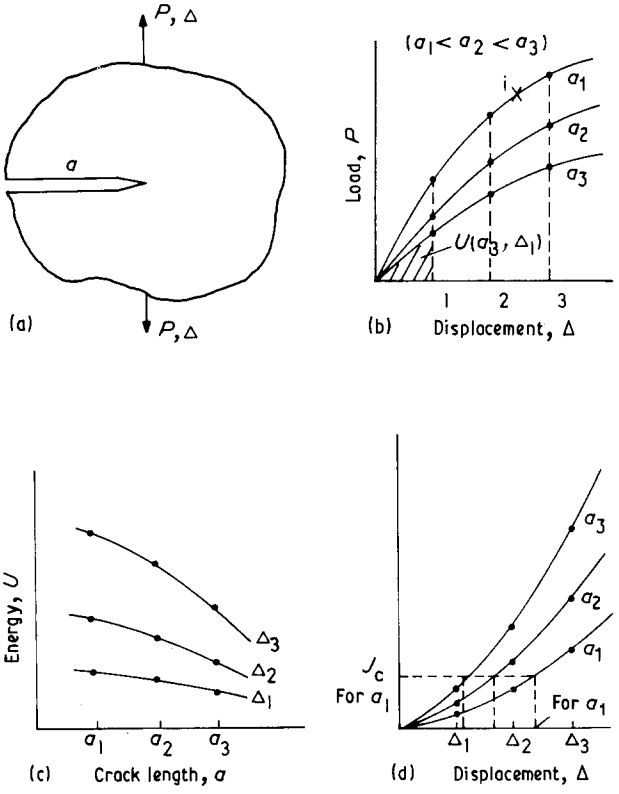

Figure 9 Schematic diagram of J against displacement evaluation. (a) Pre-cracked specimen under applied loadings; (b) Load–displacement curves of cracked specimens; (c) Stored strain energy plotted against crack length; (d) J-value plotted against displacement at constant pre-crack length.

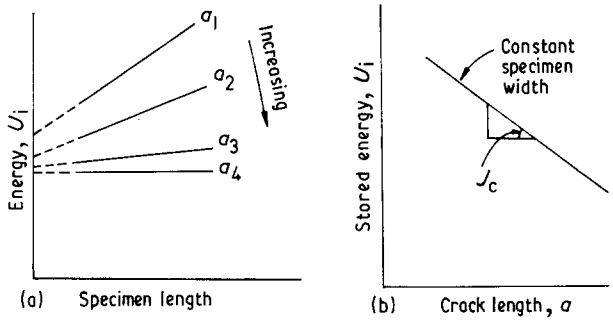

Figure 10 Schematic of the extrapolated method for J_c determination.

2.4. Quasistatic energy method

Basically, like the above mentioned extrapolation method, the quasistatic energy method attempts to separate the essential strain energy needed for fracture initiation out of the total energy absorbed in the cracked body. It is assumed that the critical J-integral value can be obtained from the following relation:

$$J_c = \frac{\int P d\Delta}{dA} \tag{12}$$

where $\int P d\Delta$ represents the area enclosed between two loading curves and the crack initiation locus and dA is the increase in crack surface area. Specifically, using the schematic load–displacement records of identical specimens which differ only in initial pre-crack length a (Fig. 11), the J_c value is evaluated as

$$J_c = \frac{1}{B} \cdot \frac{\text{Area(OEF)}}{a_4 - a_1} \tag{13}$$

where B is the specimen thickness. In other words, the triangular area (OEF) in Fig. 11 is considered by the quasistatic energy method as the essential energy required to propagate the crack from a_1 to a_4 [19–21].

3. Experimental

3.1. Test material and specimen geometry

The test material was a random short glass fibre reinforced nylon 6.6 supplied by Du Pont (commercial designation Zytel 70G 33 HS1-L). It contains 33 wt% glass fibre reinforcement with an average fibre length of 1 mm. The material was injection moulded into $220 \times 80 \times 3.2\ mm^3$ thin plates, using an end-gated mould as shown in Fig. 12. The JM12 MK11-C injection mould machine manufactured by the Cheng

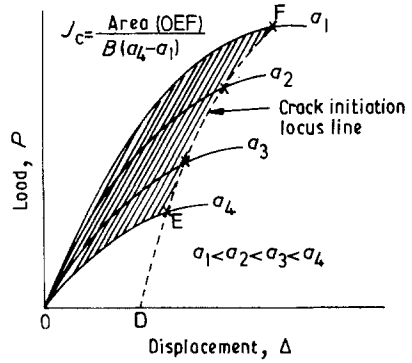

Figure 11 J_c evaluation with the area method.

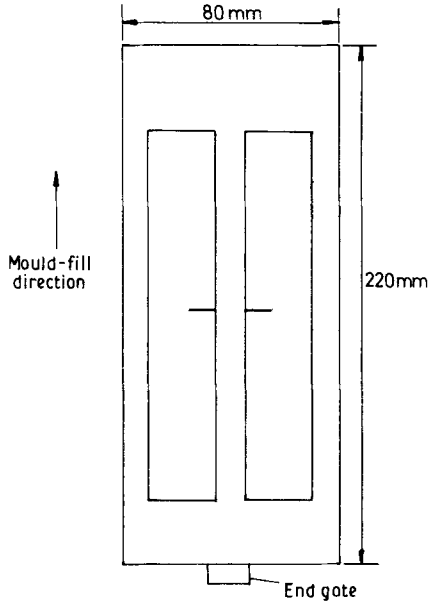

Figure 12 Geometry of injection-moulded plaques and orientation of single-edge-notched specimen.

Hsong Company was used and the injection-moulding procedures were in full accordance with the "Du Pont Glass-Reinforced Zytel Nylon Resin Moulding Guide".

A single-edge-notched specimen with a nominal width 30 mm was used in the J_c tests. Three nominal specimen lengths were selected: 64, 100 and 134 mm. Sharp notches of different lengths were machined on the otherwise identical specimens (with the same nominal specimen length). These cracks were sharpened using a sharp razor blade. Seven pre-crack lengths were chosen: 5, 7.5, 10, 12.5, 15, 17.5 and 20 mm. Three specimens for each specimen length and initial pre-crack length were prepared. This amounts to a total of 21 specimens used in the tests. In addition, standard uniaxial tension testing specimens were prepared to obtain the basic tensile stress–strain relation of this material. All specimens, including crack-growth specimens and simple tensile testing specimens, were cut out from the injection-moulded plates in such a manner that the loading direction coincided with the mould-fill direction, Fig. 12.

3.2. Experimental procedures

For J-integral measurement, the load–displacement curves were obtained by using an Instron universal testing machine, equipped with an autographic x–y recorder of load and load point displacement. A cross-head speed of 0.5 mm min^{-1} was used, being the lowest for the machine, in order to simulate a quasi-static process. All the J_c tests were performed in a displacement controlled mode, at the recorded room temperature of 20 ± 0.5 °C and relative humidity of 55 $\pm$ 5%. For positive identification of the threshold of fracture initiation, a travelling microscope of 10 magnification equipped with object-piece and eye-piece was attached to the testing machine. The basic tensile stress–strain relations of this material as a function of strain rate and temperature were recorded. As strain rate effects were found to be small for this composite, a typical room-temperature stress–strain curve shown in Fig. 6 was obtained at the strain rate of 5 mm min^{-1}.

For fractographic examination purposes, fractured specimens were carefully removed and selected regions enclosing the crack tip were then sectioned for optical or SEM observations. Crack profile and crack-tip damage were examined under a conventional reflection optical microscope. Selected testing pieces were first "cold-mounted" in epoxy and one-side surfaces of them were then polished using a 1 μm diamond paste compound with care taken to avoid any prior damage such as fibre cracking created during polishing. For SEM observations, the Cambridge stereoscan 150 scanning electron microscope operated at an accelerating voltage of 20 kV was used. In order to provide an efficient charge transfer, specimen surfaces were first sputtered with a 15–20 nm thick layer of gold-palladium.

4. Results and discussion

4.1 Load-displacement records

Basic load against load-point displacement records for specimens with different initial crack lengths and specimen lengths are shown in Figs 13 to 15. Load-displacement behaviours beyond maximum load levels are clearly revealed by these records as a consequence of the displacement-controlled loading conditions. In fact, slower, less unstable crack propagations were observed during the experiments compared with rapid crack growth under load-controlled modes. This is desirable because a clear definition of the crack initiation point plays an essential role in the determination of accurate critical J-integral value for all the three experimental techniques under study. Figs 13 to 15 indicate that sudden load drops induced by fracture initiation occur in specimens with smaller pre-crack lengths whereas fracturing processes are more gradual in specimens with longer pre-crack lengths.

Based on Figs 13–15 where points marked $\times$ indicate fracture initiation and the relation $\sigma_f = P_f/B(w - a)$ where P_f designates the fracture initiation load, the observed nominal fracture stress (σ_f) is plotted against crack length a, in Fig. 16. It is seen from Equation 8b that if J_c or ξ is assumed to be

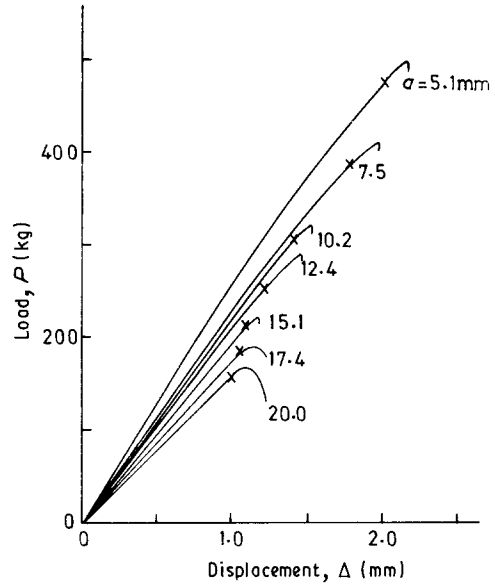

Figure 13 Load–displacement records for different pre-crack lengths and fixed specimen length of 64 mm.

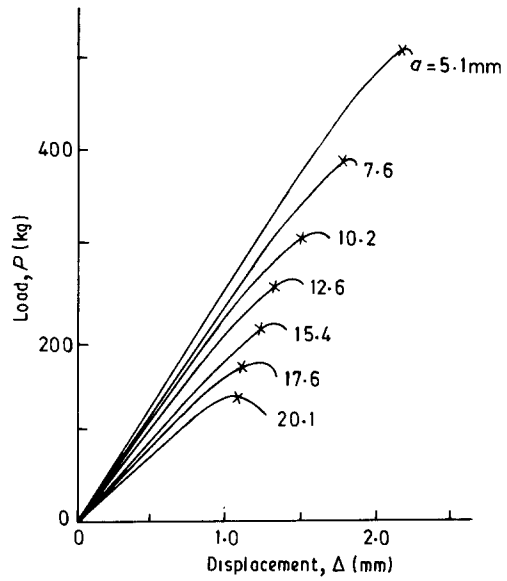

Figure 15 Load–displacement records for different pre-crack lengths and fixed specimen length of 134 mm.

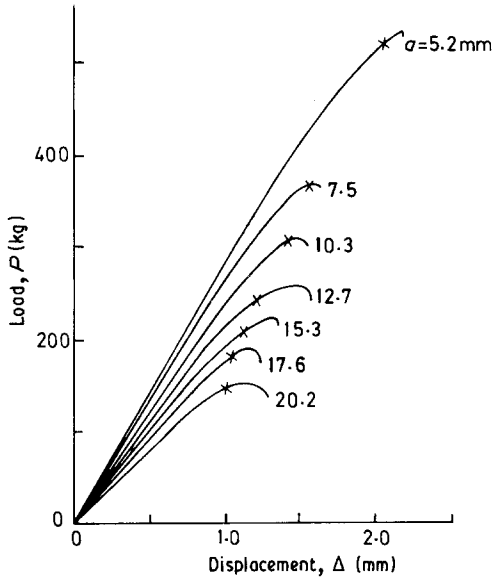

Figure 14 Load–displacement records for different pre-crack lengths and fixed specimen length of 100 mm.

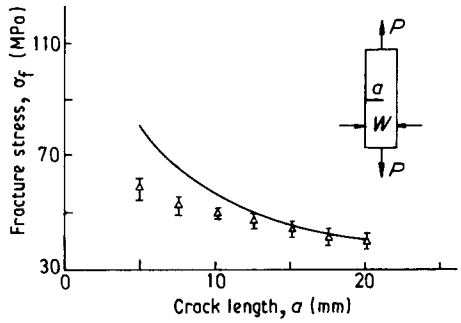

Figure 16 Comparison between experimentally measured (△) and theoretically predicted (—— from Equation 13b) fracture stresses (σ_f) for various pre-crack lengths.

material characteristic, the fracture stress (σ_f) should then be proportional to $a^{-1/2}$. If the σ_f value corresponds to the largest crack length $a = 20$ mm is accepted as the reference data, fracture stresses corresponding to smaller crack lengths can be conveniently predicted from Equation 8b as shown in Fig. 16 by the solid line. It can be seen from Fig. 16 that, when the pre-crack length a is larger than 12.5 mm or the crack length to specimen width ratio a/w exceeds 0.45, the observed fracture stresses agree well with that predicted by Equation 8b. This implies that, when the condition $a/w > 0.45$ is satisfied, the remote energy dissipation effect is of negligible significance and a constant J_c value independent of crack length and specimen geometry could possibly be obtained (see Equation 10) if an appropriate experimental technique has been adopted.

4.2. Data treatment

In accordance with the three experimental techniques introduced in the last section, the load level corresponding to load–point displacement = 0.1 mm, 0.2 mm, . . . , up to the point of crack initiation was obtained from the autographic load–displacement records shown in Figs 13 to 15. A Pascal program was written to perform necessary integrations so as to find the strain energy for a given pre-crack length and a given load–point displacement, $U(a_n, \Delta_m)$. Various values of $U(a_n, \Delta_m)$ were then plotted on strain energy U against crack length a graphs, as shown in Fig. 17. Another Pascal program was written to perform curve fitting and to calculate the gradient at desired points. Least square fitting to the U against a curves for a given load–point displacement was performed in two ways: (a) quadratic curve fitting to all experimental points and (b) linear straight line fit to the last four points corresponding to $a/w > 0.45$. As would be expected, the latter fit resulted in a constant J_c value whilst the former failed and hence was rejected. With the slope of the U against a curve at a given load–point displacement Δ, the J integral value corresponding to various Δ was then plotted as the J

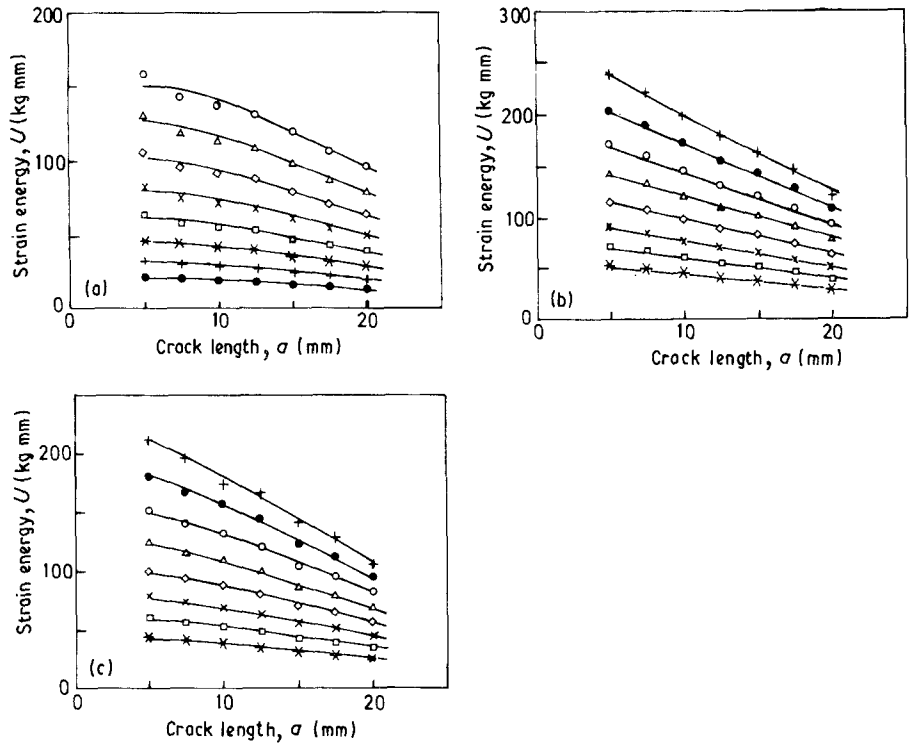

Figure 17 Strain energy absorbed by the cracked specimen as a function of pre-crack length at different load–point displacement. (a) Specimen length = 64 mm (○ △ = 1.1 mm, △ △ = 1.0 mm, ◇ △ = 0.9 mm, × △ = 0.8 mm, □ △ = 0.7 mm, × △ = 0.6 mm, + △ = 0.5 mm, ● △ = 0.4 mm.) (b) Specimen length = 100 mm (+ △ = 1.3 mm, ● △ = 1.2 mm, ○ △ = 1.1 mm, △ △ = 1.0 mm, ◇ △ = 0.9 mm, × △ = 0.8 mm, □ △ = 0.7 mm, × △ = 0.6 mm). (c) Specimen length = 134 mm (+ △ = 1.3 mm, ● △ = 1.2 mm, ○ △ = 1.1 mm, △ △ = 1.0 mm, ◇ △ = 0.9 mm, × △ = 0.8 mm, □ △ = 0.7 mm, × △ = 0.6 mm).

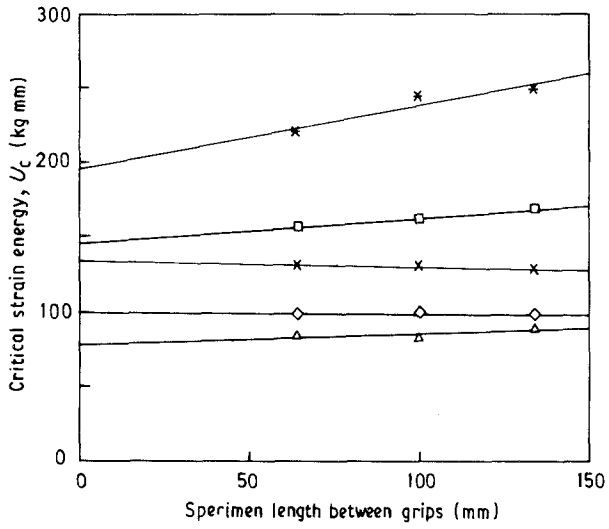

Figure 18 Critical strain energy absorbed by the pre-cracked specimen at fracture initiation as a function of specimen length for different pre-crack sizes. (* a = 10 mm, □ a = 12.5 mm, × a = 15 mm, ◇ a = 17.5 mm, △ a = 20 mm).

against Δ curve according to the schematic illustration of the compliance J determination shown in Fig. 9.

The critical J integral value, J_c, for different pre-crack lengths was finally found from the J against Δ curve if the corresponding critical load–point displacement, Δ_c, had been obtained from the autographic load–displacement record.

As to the J_c evaluation based on the quasistatic energy method, the same U values computed from the Pascal program were used at different crack increments. For the extrapolation method, the critical strain energy U_c for different specimen lengths was obtained by using the U against Δ output from the first Pascal program. This furnished the U against specimen length l graph shown in Fig. 18. Extrapolation of a straight line in Fig. 18 corresponding to a given pre-crack length resulted in an intercept on the ordinate, i.e., U_c (l = 0), which is considered by the extrapolation method as the essential energy absorbed in the crack tip region. Then, if possible, J_c was obtained by finding the slope of the U_c (l = 0) against a plot.

4.3. Discussion

The critical J-integral values obtained from compliance J-determination and quasistatic energy method are shown in Fig. 19a and b, respectively, as functions of pre-crack length to specimen width ratio (a/w). Clearly, when $a/w > 0.45$, the J_c value obtained from both methods can be regarded as a constant independent from pre-crack length and specimen length. Under such conditions, the load level at fracture initiation was small* and hence possibly did not cause much

* Experimentally, it was found that, for a fixed specimen length of 100 mm and specimen width of 30 mm, fracture initiation loads corresponding to two pre-crack lengths, 5 and 15 mm, were 520 and 210 kg, respectively. Nominal fracture stresses acting on the specimen cross-section areas were 53 and 21 MPa, respectively. Recalling that the yield stress of the material σ_0 = 40 MPa, one could see that general material damage would have occurred before the crack started to propagate in the former case but not in the latter one.

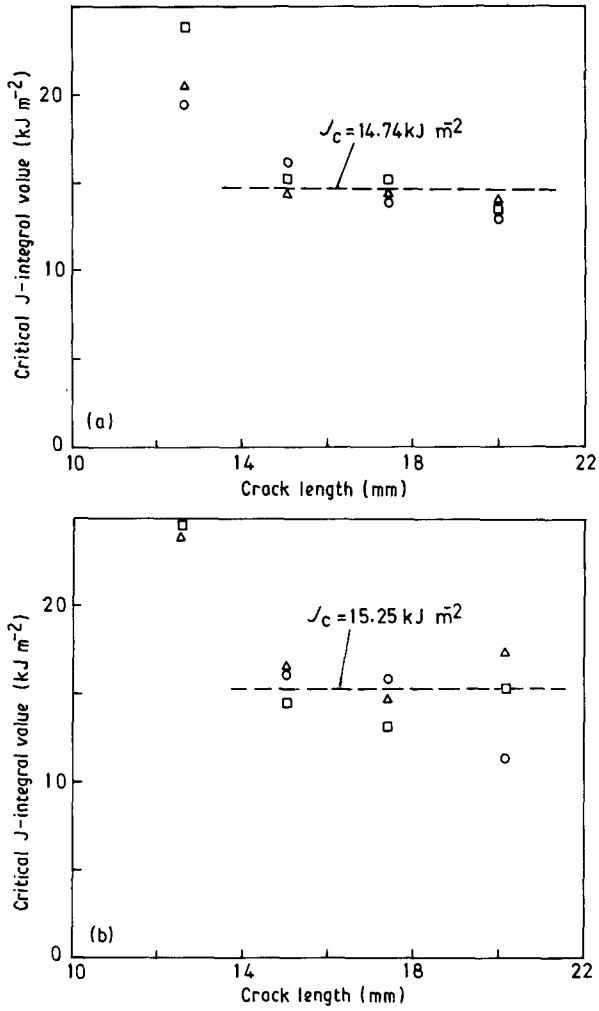

Figure 19 J_c values obtained by using (a) compliance calibration method and (b) area method. Specimen length (○ l = 64 mm, △ l = 100 mm, □ l = 134 mm). Specimen width = 30 mm.

general material damage away from the crack tip region, i.e., the far field effect was limited and negligible. Energy absorbed by the material body was predominantly dissipated through various damaging mechanisms in the localized crack tip region as well as the formation of new crack surface areas. When precrack length was, however, short, it was expected that the high level of applied load would cause substantial damage in the material at large (microcracking, debonding, etc.) which increased the total energy absorbed at crack initiation. For too short a crack length, the J-integral value found would be greater due to the remote energy dissipation and possibly it did not represent the J_c value as material property. Consequently, for the least square fit of strain energy against crack length curves, only those data corresponding to long precrack lengths ($a/w > 0.45$) were used.

From Fig. 19a and b, it is observed that the quasistatic energy method gives satisfactory results as compared with those from the standard compliance calibration method. Compared with the tedious compliance calibration method, the quasistatic energy method which has been used extensively in the past by Chow *et al.* [18–23] and Kim and Joe [16, 17, 33] is simpler and physically appealing. This can be best clarified by re-examining the physical implication of the J-integral under brittle fracture in which $J = G$, with G signifying Irwin's elastic strain energy release rate. Rice [11] has pointed out that the J-contour integral can be alternatively defined as

$$J = -\frac{dU}{dA} \tag{14}$$

where $U(a)$ denotes the potential energy of the system as a sum of the elastic strain energy in the cracked body and in the loading mechanisms (see also Equation 1). Unfortunately, generalization of the energetic interpretation for the J-integral through Equation 14 cannot be proved if the path-independent property of J persisted. Indeed, for the plane infinite sheet with a central crack subjected to uniform remote biaxial loadings (Fig. 20), it can be shown [34, 35] that if a crack extends from both crack ends under "fixed-grip" conditions

$$-\left.\frac{dU}{dA}\right|_{\substack{\text{fixed}\\ \text{grip}}} = -2\zeta\frac{K^2}{E} = -2J = -2G \tag{15}$$

whereas for "dead load" crack extension from both crack ends,

$$-\left.\frac{dU}{dA}\right|_{\substack{\text{dead}\\ \text{load}}} = 2\zeta\frac{K^2}{E} = 2J = 2G \tag{16}$$

with $\zeta = 1$ for plane stress and $\zeta = 1 - \nu^2$ for plane strain. On the other hand, when there are no boundary constraints on the cracked body,

$$-\frac{dU}{dA} = \frac{[1 + k(2 - \kappa)](1 + \nu)}{2}\cdot\frac{K^2}{E}$$

$$\neq \begin{cases} -\left.\dfrac{dU}{dA}\right|_{\substack{\text{fixed}\\ \text{grip}}} \\ -\left.\dfrac{dU}{dA}\right|_{\substack{\text{dead}\\ \text{load}}} \end{cases} \tag{17}$$

and this is true even in the case where no loads parallel to the crack line are applied. In Equation 17, k represents the load biaxiality (Fig. 20) and $\kappa = (3 - \nu)/(1 + \nu)$ for plane stress, $(3 - 4\nu)$ for plane strain. Using the line integral expression for J, however, the J-integral value has been proved [36, 37] to be independent of the load biaxiality k. Consequently, the

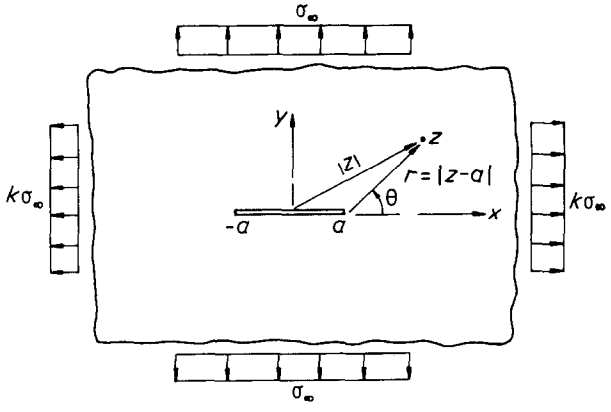

Figure 20 Geometry and boundary tractions of a biaxially loaded centre-cracked plane sheet.

energy-based interpretation of J through Equation 14 must be limited to the two special boundary constraint conditions of Equations 15 and 16. In other words, the J-integral *per se* is "of more mathematical consequence than physical" and it cannot be extended arbitrarily to circumstances where it fails to be representative of the total potential energy fluctuations caused by crack extension. In view of Equation 17, there certainly exists a possibility in that, as the crack extends, the potential energy of the entire cracked body remains unchanged during the course if the load biaxiality factor k is chosen such that it approaches $1/(\kappa - 2)$ in value.

We notice that, whilst the compliance calibration method and the extrapolation method depend strongly on the energetic definition of J through Equations 15 or 16, the quasistatic energy method estimates the fracture toughness value more directly and naturally in that no boundary constraint is necessitated in the course of crack extension. It would be less confusing, therefore, if the fracture toughness obtained by using the quasistatic energy method had not been labelled as "J_c" but with some other parameter like $\tilde{G}_c$. In the present paper, although the notion "J_c" is retained for the quasistatic energy method in order to keep to the common practice in this field, it is understood that its physical meaning is different from that of the critical J-integral value. It is believed that it is the virgin contour integral expression endowed with a complex analytic structure which made many people confer a high status on J as a fracture parameter and label their result as "J_c" even though their estimate of $-\mathrm{d}U/\mathrm{d}a$ did not satisfy either of the two boundary constraint conditions of "fixed-grip" and "dead load".

On the other hand, though the quasistatic energy method is simple and physically more appealing, it is more prone to error due to the difficulties of calculating accurately the area enclosed by the loading curves and the crack initiation locus. In fact, the crack initiation locus has not yet been well defined and in our case, it is approximated by piecewise linear straight lines joining the "$\times$" marked crack initiation points. Furthermore, the crack initiation point is difficult to be defined accurately just by observation and empirical judgement, even when the lowest crosshead speed (0.5 mm min^{-1}) has been used throughout the test. It is impractical, however, to use paint or ink so that enhanced observation may be achieved as it has been reported [38] that for nylon, even water can cause stress induced cracking. To make the situation less ambiguous, some more advanced experimental techniques such as acoustic emission or potential drop method should be employed to give a more accurate identification of the crack initiation locus line.

As to the extrapolation method introduced by Agarwal *et al.* [14], it can be observed from Fig. 18 that, the extrapolated strain energies to the zero specimen length for the five pre-crack lengths cannot result in a straight line like that of Fig. 10b. In fact, as only those data corresponding to $a/w > 0.45$ are accepted as being valid, it is difficult, if not impossible, to employ eye-fitting extrapolation to find the strain energy absorbed by a pseudo zero length specimen. Apart from its questionable physical interpretation, there seems to be no explicit advantages in terms of time and effort for recommending the extrapolation method as an alternative experimental technique.

5. Conclusions

The conclusions are as follows.

1. Plane-stress fracture toughness of a short glass fibre reinforced injection-moulded nylon 6.6 has been evaluated using a single-edge-notched tension type specimen. It is found that, even though the condition of linear elastic fracture mechanics has generally been violated, a constant J_c value independent of pre-crack length as well as specimen geometry can still be obtained if the crack length to specimen width ratio (a/w) is sufficiently large so that energy dissipation due to remote damage mechanisms is of negligible significance.

2. J_c values based on three different experimental techniques, although all three of them depend essentially on the energetic interpretation of the J integral, are obtained and compared.

3. The compliance calibration method yields a J_c value of 14.74 kJ m^{-1} whereas the J_c value furnished by the quasistatic energy method, of 15.25 kJ m^{-1}, is slightly larger but acceptable. The extrapolation method, on the other hand, cannot give physically consistent J_c values, in addition to its questionable theoretical representation.

4. It is argued that the quasistatic energy method is established on a more representative physical foundation as no constraint on boundary conditions is necessitated during the course of crack extension.

References

1. S. K. GAGGAR and L. J. BROUTMAN, *Fibre Sci. Tech.* **9** (1976) 205.
2. *Idem.*, ASTM STP 631 (American Society for Testing and Materials, Philadelphia, 1977) pp. 310–330.
3. M. J. OWEN and P. T. BISHOP, *J. Compos. Mater.* **7** (1973) 146.
4. R. M. ALEXANDER, R. A. SCHAPERY, K. L. JERINA and B. A. SANDERS, ASTM STP 772 (American Society for Testing and Materials, Philadelphia, 1982) pp. 208–224.
5. T. M. MOWER and V. C. LI, *Engng Frac. Mech.* **26** (1987) 593.
6. J. F. MANDELL, D. D. HUANG and F. J. MCGARRY, ASTM STP 772 (American Society for Testing and Materials, Philadelphia, 1982) pp. 3–32.
7. J. KARGER-KOCSIS and K. FRIEDRICH, *J. Mater. Sci.* **22** (1987) 947.
8. A. A. GRIFFITH, *Phil. Trans. R. Soc.* **A211** (1921) 163.
9. *Idem., ibid.*, **A221** (1920) 163.
10. J. EFTIS and H. LIEBOWITZ, *Engng Frac. Mech.* **7** (1974) 101.
11. J. R. RICE, *J. Appl. Mech.* **35** (1968) 379.
12. T. A. BEGLEY and J. D. LANDES, ASTM STP 514 (American Society for Testing and Materials, Philadelphia, 1972) pp. 1–20.
13. *Idem.*, ASTM STP 632 (American Society for Testing and Materials, Philadelphia, 1977) pp. 57–81.
14. B. D. AGARWAL, B. S. PATRO and P. KUMAR, *Engng Frac. Mech.* **19** (1984) 675.

15. R. K. SINGH and K. S. PARIHAR, *J. Mater. Sci.* **21** (1986) 3921.
16. B. H. KIM and C. R. JOE, *Engng Frac. Mech.* **30** (1988) 493.
17. *Idem., ibid.* **32** (1989) 233.
18. C. L. CHOW, J. WANG and P. N. TSE, *Tire Sci. Technol.* **16** (1988) 44.
19. C. L. CHOW and K. M. NGAN, *J. Strain Anal.* **12** (1977) 45.
20. *Idem, Int. J. Frac.* **14** (1978) 277.
21. C. L. CHOW, *J. Strain Anal.* **17** (1982) 67.
22. C. L. CHOW and P. M. LAM, *J. Engng Mater. Technol.* **96** (1974) 41.
23. C. L. CHOW and K. M. NGAN, *J. Strain Anal.* **13** (1978) 115.
24. H. W. LIU, ASTM STP 381 (American Society for Testing and Materials, Philadelphia, 1964) pp. 23–26.
25. *Idem., Engng Frac. Mech.* **17** (1983) 425.
26. R. M. McMEEKING and D. M. PARKS, ASTM STP 668 (American Society for Testing and Materials, Philadelphia, 1979) pp. 175–194.
27. J. W. HUTCHINSON, *J. Mech. Phys. Solids* **16** (1968) 13.
28. J. R. RICE and G. F. ROSENGREN, *J. Mech. Phys. Solids* **16** (1968) 1.
29. W. L. HU, A. S. KUO and H. W. LIU, in Proceedings of the 12th Annual Meeting of Soc. of Engng. Sci. Austin, TX, 1975.
30. W. L. HU and H. W. LIU, in Proceedings of the 2nd International Conference on Mechanical Behavior, Boston, MA, 1976.
31. H. W. LIU and T. ZHUANG, *Theor. Appl. Frac. Mech.* **7** (1987) 149.
32. T. ZHUANG and H. W. LIU, *Int. J. Frac.* **27** (1985) R87.
33. B. H. KIM and C. R. JOE, *ibid.* **34** (1987) R57.
34. J. EFTIS and D. L. JONES, *ibid.* **20** (1982) 267.
35. J. EFTIS, *Engng Frac. Mech.* **26** (1987) 567.
36. J. R. RICE, *J. Mech. Phys. Solids* **22** (1974) 17.
37. J. EFTIS, N. SUBRAMONIAN and H. LIEBOWITZ, *Engng Frac. Mech.* **9** (1977) 189.
38. L. H. LARSSON, in "Advances in Elasto-Plastic Fracture Mechanics" (Elsevier Applied Science Publishers, London, 1979) pp. 69–73.

Received 29 June 1989
and accepted 6 March 1990